Journal of Radioanalytical and Nuclear Chemistry (2021) 327:159–173
https://doi.org/10.1007/s10967-020-07481-2

Synthesis and characterization of chitosan–vermiculite composite beads for removal of uranyl ions: isotherm, kinetics and thermodynamics studies

Zeynep Mine Şenol[1] · Selçuk Şimşek[2] · Ali Özer[3] · Dilek Şenol Arslan[4]

Received: 16 July 2020 / Accepted: 23 October 2020 / Published online: 19 November 2020

Abstract
In this study, a new material containing Chitosan (Ch)–Vermiculite (V) composite beads was synthesized with epichlorohydrin cross-linking agent and used to remove uranyl ions from the aqueous solution. The prepared new material was characterized by SEM, XRD, FTIR analyses and PZC measurement. The effects of significant parameters on adsorption including temperature, pH, concentration and time were investigated. The obtained results indicated that the new composites of Ch–V was revealed in different structure. The zeta potential analyses showed that electrostatic attraction existed during the adsorption process between the uranyl ions and Ch–V. The maximum adsorption capacity of material was calculated as 0.665 mol kg^{-1} by considering Langmuir equation. Adsorption kinetic was also explained with pseudo second order and intra particular diffusion models. Experimental studies clearly showed that the adsorption was endothermic and occurred spontaneously. The newly developed smart material has many advantages such as reusability, high adsorption capacity, selectivity and economics.

Keywords Chitosan · vermiculite · UO_2^{2+} · Wastewater treatment · adsorption

Introduction

Uranium is a radioactive element which is so rare in nature. It exists mostly in the form of hexavalent uranyl ions in the solution phase, which is dangerous for human and environmental health. Removal/recovery of the uranyl ions in the solution phase is important both in terms of health and use as nuclear fuel and raw material in many industries. Once taken into the body, their toxic effects accumulate in specific organs then they lead to organ failure and death [1]. Therefore, wastewater and drinking water must be removed from them to make it safe.

Several physicochemical *methods* can be utilized for the removal of pollutants from the aqueous phase and the recovery of precious metals [2]. However, some of these methods are not preferred because of their difficulty of use and high cost. Among these methods, adsorption/solid phase extraction is the most preferred methods due to various aspects [3]. Especially, ease of use, suitable adsorbent design and inexpensiveness are some of the reasons to be preferred. In the metal removal studies, the design and use of suitable functional group-bearing adsorbents, re-usability of adsorbents and a type of specific adsorbent design are some of the advantages why adsorption is preferred.

Hybrid adsorbents [4] which were prepared from materials such as natural minerals [5], clays [6], natural and synthetic polymers [7, 8], are the most studied ones among the adsorbents in recent years. Composite materials come into prominence as adsorbent by combining the properties of the materials in interest. Studies in recent, especially composite materials formed by polymers as matrix and clay or minerals as adsorbent which are widely used in the removal of metals from aqueous solutions [9]. New structures are formed by

✉ Zeynep Mine Şenol
msenol@cumhuriyet.edu.tr

1 Department of Food Technology, Sivas Cumhuriyet University, 58140 Sivas, Turkey

2 Department of Chemistry, Sivas Cumhuriyet University, 58140 Sivas, Turkey

3 Department of Metallurgical and Materials Engineering, Sivas Cumhuriyet University, 58140 Sivas, Turkey

4 Department of Materials Science and Nanotechnology Engineering, Abdullah Gül University, Kayseri, Turkey

the large surface area of the clays and the functional group bearing polymers on this area are preferred with relatively high recovery capacity and high recovery rate for adsorption [10].

Vermiculite is one of the most studied minerals among clay minerals. It is alumina silicate mineral, which has two octahedral and one tetrahedral structure 2:1 (T-O-T layer structures). Due to the interchangeable cations such as K^+, Ca^{2+} Mg^{2+} are located between the layers, it is used for metal adsorption studies. But, some studies have shown that, its adsorption capacity is lower than most metals [11].

Chitosan is a natural polymer with a wide range of application areas. With its unique properties, it is often preferred in many composite materials structure. For example, it has found application in many fields, such as membrane, coating, binder and controlled release of drug and agricultural purposes, and etc. [12]. Together with the reactive nitrogen and hydroxyl groups in its structure, especially the complex structures with metals make it a potential adsorbent. The chitosan dissolves under the acidic conditions, although it does not have solubility in alkaline and neutral conditions. So, this condition limits the use of chitosan as an adsorbent. But, it can possible to use chitosan as an adsorbent with modification or generated composites [13].

Chitosan–vermiculite composites were prepared by different methods and used for various heavy metal uptake [14–17]. From these literature reports, it is observed that the investigations on exposing the potential for heavy metal adsorption are still scanty and inadequate. In addition, to the best of our knowledge, a detailed research report about the adsorption of uranyl ions onto chitosan-vermiculite composite as sorbents is not available in the literature. In this study, chitosan-vermiculite composite beads were synthesized using epichlorohydrin and tripolyphosphate as cross-linked agent in order to obtained adsorbent applicable for uranyl ions from aqueous environments. The characterizations of the new synthesized adsorbent were performed by FT-IR SEM–EDX, XRD, and point of zero charge (PZC) analyses in detail. Adsorption properties were investigated for hexavalent uranyl ions from aqueous environment. The effect of concentration, pH, and temperature and contact time on adsorption were considered and optimum conditions were determined.

Experimental

Reagents and equipment

In order to examine the adsorption of UO_2^{2+} ions onto the Ch–V, $(CH_3COO)_2UO_2.2H_2O$ and 4-(2-pyridilazo) resorcinol (PAR) and other chemicals were obtained from Merck (Germany). Distilled water was used in all experiments. The uranyl concentration was determined using a UV–vis spectrophotometer (SHIMADZU, 160 A model, Japan). This spectrophotometer has a wavelength range of 190–1100 nm and has a resolution of ± 0.2 nm. FT-IR analysis was recorded using the FT-IR spectrophotometer (Perkin Elmer 400) in order to examine the functional groups in the range of 400–4000 cm^{-1} with KBr pellets. The surface morphology of the samples was observed with a scanning electron microscope (TESCAN MIRA3 XMU, FEG-SEM, Brno, Czechia) equipped with an energy dispersive spectrometer (EDX) attachment. A pH meter (Selecta, Spain) was used to measure the pH values with a glass-calomel electrode. Centrifuge (Hettich Universal) was used to accelerate phase separation. A thermostatically controlled water bath (Nuve NT120, Turkey) was used to keep the temperature constant.

Synthesis of Ch–V composite beads

To synthesize about 4 g of Ch–V composite, 2 g of chitosan and 2 g of vermiculite were mixed in a 5% (v / v) acetic acid solution for 2 h until a homogeneous mixture was obtained. Then a solution of epichlorohydrin (ECH) was added and stirring was continued. Then the mixture was added dropwise to the sodium tripolyphosphate (NaTPP) solution to form composite beads. The resulting beads were washed with distilled water until the conductivity of the wash water reached approximately pure water conductivity as well as neutral pH value. The samples were dried in the oven at 40 ^{0}C and ground to a grain size of 50 mesh and stored in closed containers for later use.

Batch adsorption procedure

Adsorption experiments were performed by using batch method. The effect of concentration, kinetic (time), thermodynamic (temperature) and recovery were investigated in terms of pH. Stock UO_2^{2+} solution (5000 mg L^{-1}) was prepared using distilled water. All experiments were carried out at a shaking rate of 140 rpm in 10 mL polypropylene tubes containing 100 mg adsorbent at constant concentration of 1000 mg L^{-1} (3.7×10^{-3} mol L^{-1}) UO_2^{2+} in 10 mL solutions. To examine the effect of pH, the variety of initial pH values (pH: 1–7) in the fixed concentration of UO_2^{2+} solutions were used. In order to investigate the effect of initial metal concentration, the experiments were carried out by adding 50–2000 ppm ($(0.18–7.4)\times10^{-3}$ mol L^{-1}) UO_2^{2+} to the mentioned solutions. The kinetic studies were performed by using 30 mL solutions at a constant concentration of UO_2^{2+} ions containing 300 mg of Ch–V. The thermodynamic studies were done at five different temperatures of UO_2^{2+} solutions. The concentration of UO_2^{2+} was determined by the absorbance measurement and by using the PAR method [18]. In this method, concentration of UO_2^{2+} ions are formed

spectrophotometrically as a selective complex with PAR at λ = 530 nm. Q (mol kg^{-1}) was calculated with equation given Table 1. In addition, all equations and parameters used in adsorption model calculations were presented in Table 1.

Results and discussion

Characterization

FT-IR analysis

The FT-IR spectra of the V, Ch and Ch–V composites are given in the Fig. 1. When the vermiculite spectrum was examined, it is observed that the band at 456 cm^{-1} is assigned to Si–O groups, the band at 673 cm^{-1} is correspond to Al–O band, and the peak at 962 cm^{-1} is assigned to the bands of Si–O, which are characteristic peaks for vermiculite [19]. Additionally, the wide band between the wavelengths of 1640–3400 cm^{-1} is assigned to the H–O–H and OH groups. In the FT-IR spectra, bands between 3290–3350 cm^{-1} are associated with the OH and NH groups and 2864 cm^{-1} is observed characteristic Ch peak. Peaks corresponding to the 1650 and 1575 cm^{-1} wave numbers correspond to amide C–O and amide N–H groups, 1070 cm^{-1} attributed to the C–O bond which are characteristic peaks for Ch. When the FT-IR spectrum of Ch–V composite is examined, it is seen that it is different from both spectra. Although the characteristic peaks of both components are observed in the spectrum of the composite, in particular the further expansion of the peak in the range of 900–1100 cm^{-1} is evident that the overlap of the peaks of both components occurred in this wave number.

Table 1 Mathematical equations

Model	Equation	Parameters
	$Q = \left[\frac{(C_i - C_e)V}{w}\right]$	
Isotherm		
Langmuir	$Q_e = \frac{Q_L K_L C_e}{1+K_L C_e}$	Q_L, K_L
Freundlich	$Q_e = K_F C_e^n$	K_F, n
Dubinin-Raduskevich	$Q_e = X_{DR} e^{-K_{DR}\varepsilon^2}$	X_{DR}, K_{DR}
Kinetic		
Pseudo first order	$Q_t = Q_e[1 - e^{-k_1 t}]$	k_1, Q_e
Pseudo second order	$Q_t = \frac{t}{\left[\frac{1}{k_2 Q_e^2}\right]+\left[\frac{t}{Q_e}\right]}$	k_2, Q_e
Intraparticle diffusion	$Q_t = k_i t^{0.5}$	k_i
Thermodynamics		
The free energy of adsorption	$\Delta G^0 = -RT\ln K_L$	ΔG
Vant Hoff	$\ln K_L = \frac{\Delta S^0}{R} - \frac{\Delta H^0}{RT}$	ΔH, ΔS

C_i and C_e are the initial and equilibrium concentrations (mol L^{-1}), w is the mass of adsorbent (kg) and V is the solution volume (L). Q_e: The adsorbed amounts at equilibrium (mol Kg^{-1}),), Q_t: The adsorbed amounts at time t (mol Kg^{-1}), Q_L: Langmuir monolayer adsorption capacity (mol Kg^{-1}),), K_L: Langmuir adsorption equilibrium constant (L mol^{-1}), K_F: Freundlich constants (mol Kg^{-1}), n: Intensity of adsorption (n represents the heterogeneity of the adsorptive surface), K_{DR}; DR constant related to the sorption energy (mol^2 K J^{-2}), X_{DR}: DR adsorption capacity (mol kg^{-1}), ε: Polanyi potential given with $\varepsilon = RT\ln(1 + \frac{1}{C_e})$, R: Ideal gas constant (8.314 J mol^{-1} K^{-1}), T: absolute temperature (298 K), Free energy change (E; kJ mol^{-1}) required to transfer one mole of ion from the infinity in the solution to the solid surface was then derived from $E = (2K_{DR})^{-1/2}$. k_1, k_2 and k_i are the rate constants, Initial adsorption rate (H) for pseudo-second-order is also calculated from $H = k_2 Q_e^2$

SEM–EDX analysis

Figure 2 represents the chitosan flakes and surface morphology imaged by SEM in secondary electron mode. It can be seen that, chitosan polymer forms in individual flakes as leaves and surface is rather rough by the evaporation of water or hydroxyl ion absorbed species after drying even after low vacuum. The inset picture shows a closer look to rough surface.

Figure 3 shows the vermiculite in as received condition prior to experiments. The inorganic material is characterized by smooth surface and layered structure which gives opportunity to expand after chemical processes that can be monitored by XRD. The layers can easily see at lower magnification as well as the inset image at higher magnification. The vermiculite is also seen that it was deformed to fragment into smaller and finer particle while transporting, that are deposited onto the surface that was resulted from hydroxylated nature of mineral and relative humidity of environment. This weak bonding can be classified as Van der Waals short range bonding which may release the fragmented and layered particles in water.

Figure 4 shows the intercalation of chitosan polymer into interlayers of vermiculite mineral after wet chemical process. These images were taken in secondary electron imaging mode, moreover by the aid of back scattered electron imaging of SEM as seen in lower inset image, polymers can be named as the darker regions due to lower atomic density (1–1.2 g/cm^3) while the lighter regions were labeled as vermiculite as to be higher atomic density varies depending on the Ca–Al–Si–Mg cation ratio (2.5–2.8 g/cm^3). The thin arrows in bigger image as well as upper inset picture show the polymer intercalation between the mineral layers by expanding the structure by hydroxyl (OH^-) groups.

Figure 5 demonstrates the uranium oxide adsorption/embedding into vermiculite-chitosan composites. The electron microscopy imaging was performed with back scattered electron imaging for ease of evaluation of atomic density distribution. Since the Rutherford scattering comes from electrons interacted with the nucleus of atoms, more the

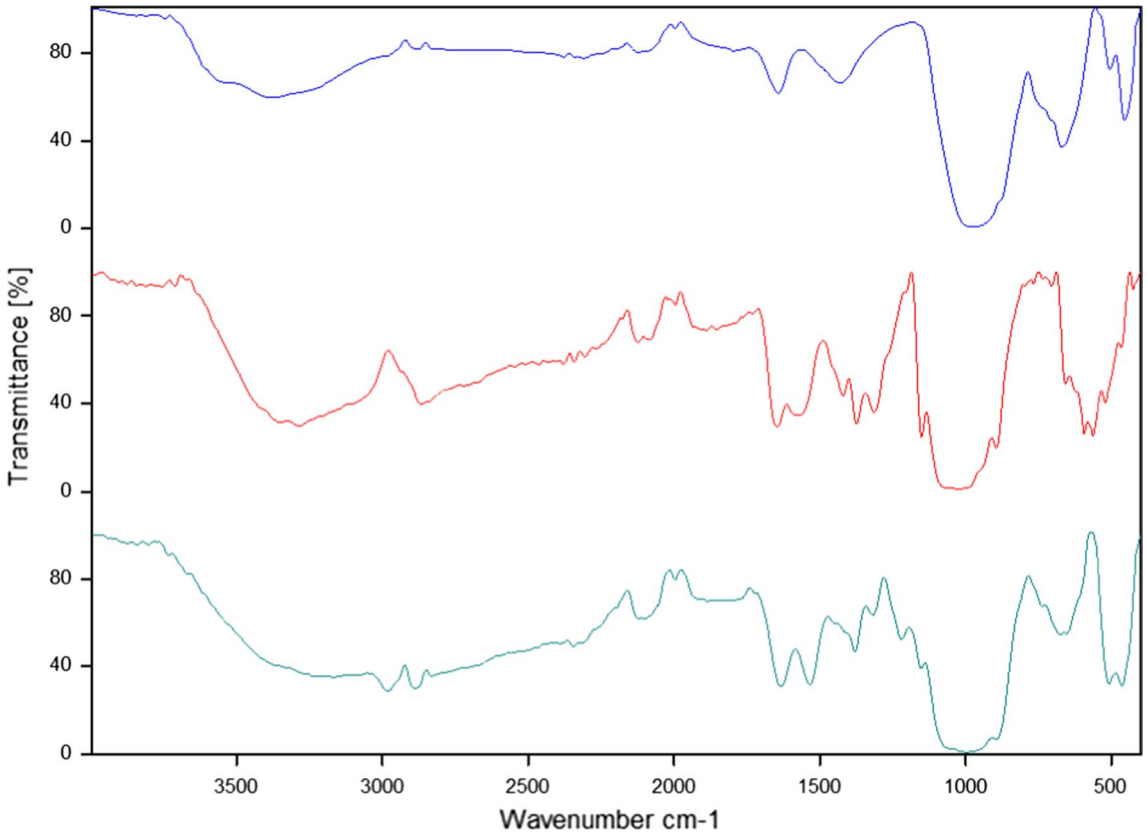

Fig. 1 FT-IR spectra of Ch, V and Ch–V composite. (blue: Vermiculite, red: Chitosan, green: Ch–V)

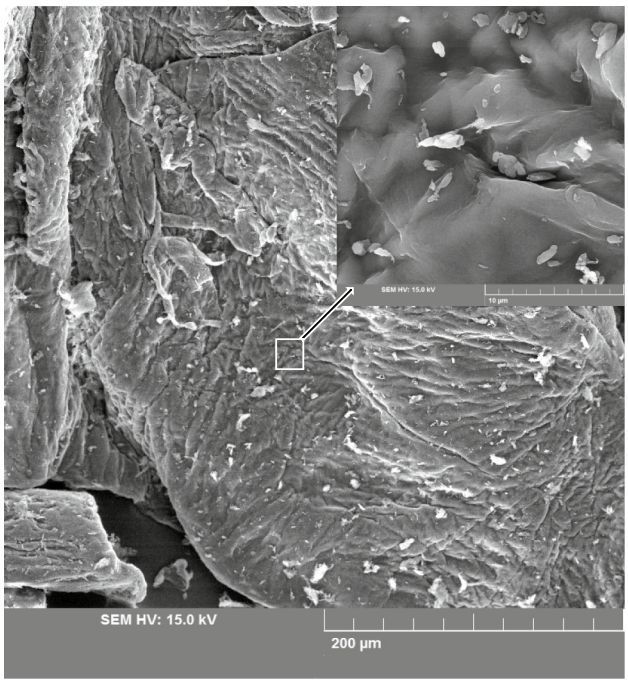

Fig. 2 SEM image of pure Chitosan

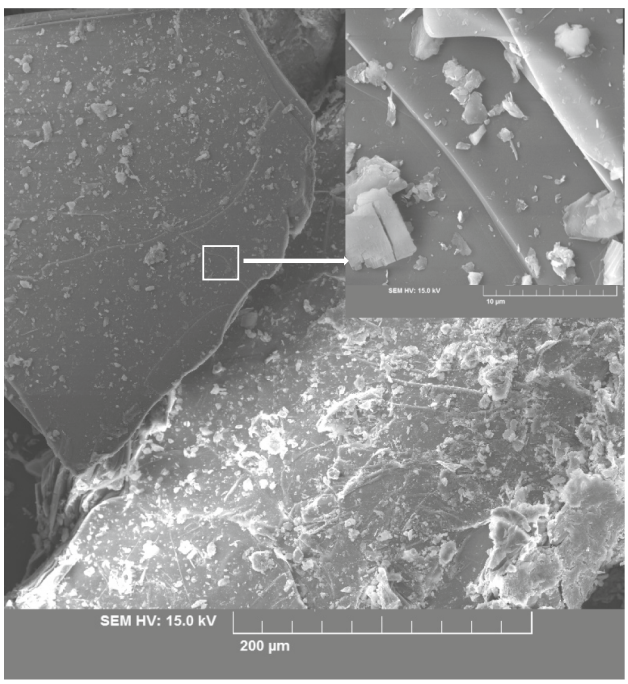

Fig. 3 SEM image of pure Vermiculite

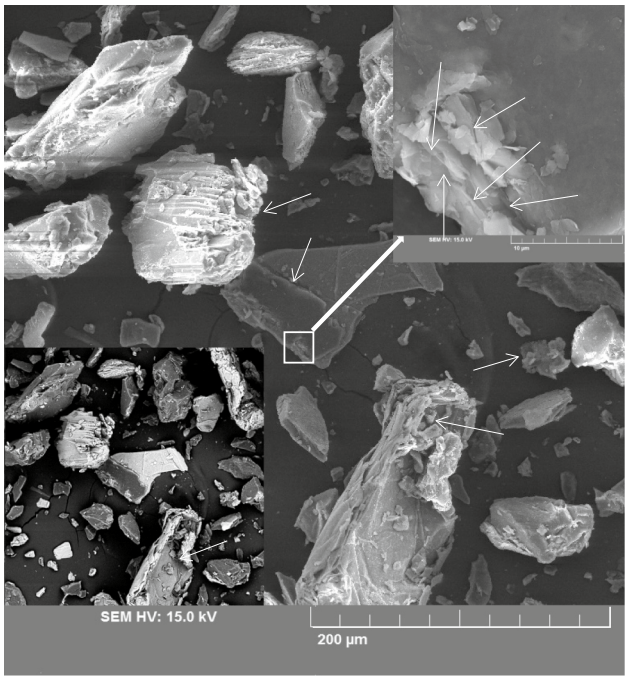

Fig. 4 SEM image of Ch–V composite

electrons hit the bigger atoms (denser regions), the more the scattered and counted electrons by detector and are seen lighter than low density atomic regions. The particles about 1 micron and smaller as illustrated by black arrows indicate the U containing oxides. Half penny like U containing particles was believed to be grown from wet precipitation which resulted from needle like particles as shown with arrows. The Energy Dispersive X-ray spectrum was also given to approve the U peak at a certain concentration on surface. This cooperation of U with mineral and chitosan may be due to the OH^- groups of vermiculite associated with NO_x and OH^- groups of chitosan reacted with UO_2 and other U–O complexes.

Figure 6a represents the SEM-BSE image of the composite doped with U. The U mapping is shown in Fig. 6b that presents the U rich areas in green both in ceramic phase and polymer adjuncts. As illustrated in Fig. 6b, the U was absorbed by chitosan as polymer and vermiculite as ceramic phase. Figure 6c is the spectrum of area with U adsorption.

Ceramic phase is evident with the Ca, K, Mg, Al, Si, Na peaks in related eVs. Moreover, C peaks overlaid with Ca and K peaks at lower keVs, N and P also comes from the chitosan as well as oxygen coming both from the vermiculite and chitosan. U has high intensity peaks which means to higher amount of U (Mα) adsorption on the area of interest. Since the C comes from all over the stub and chitosan itself, it was removed from the quantification list not to suppress the quant of other related elements. Element list was shown in Fig. 6d corresponding to SEM images and spectrum in Fig. 6c. One can clearly understand that U was all over the inorganic phase meant to an adsorption at the layers and pores of ceramic.

XRD analysis

Figure 7 shows the XRD data drawn for chitosan, vermiculite, chitosan-vermiculite and chitosan-vermiculite-UO_2 polymer-ceramic composites. Figure 7a represents an amorphous chitosan structure. The characteristic hump around 15° and 25° (2 thetas) mean that any crystalline structure with peaks isn't present. Figure 7b is the pattern for vermiculite with pseudo-nano sized primary crystallite size of 77 Å ± 7 Å measured from 5 main peaks at 25°, 28°, 33°, 44° and 58° (2 thetas). This was found out by Scherrer equation described elsewhere [19, 20] following the pseudo-Voigt function and Constant FWHM estimation

Fig. 5 SEM images of uranyl adsorbed Ch–V composite. {$[UO_2^{2+}]_0$: 1000 mg L^{-1}, adsorbent dosage: 100 mg, V:10 mL, natural pH: 4.0–4.5, contact time: 24 h, temperature: 25 °C}

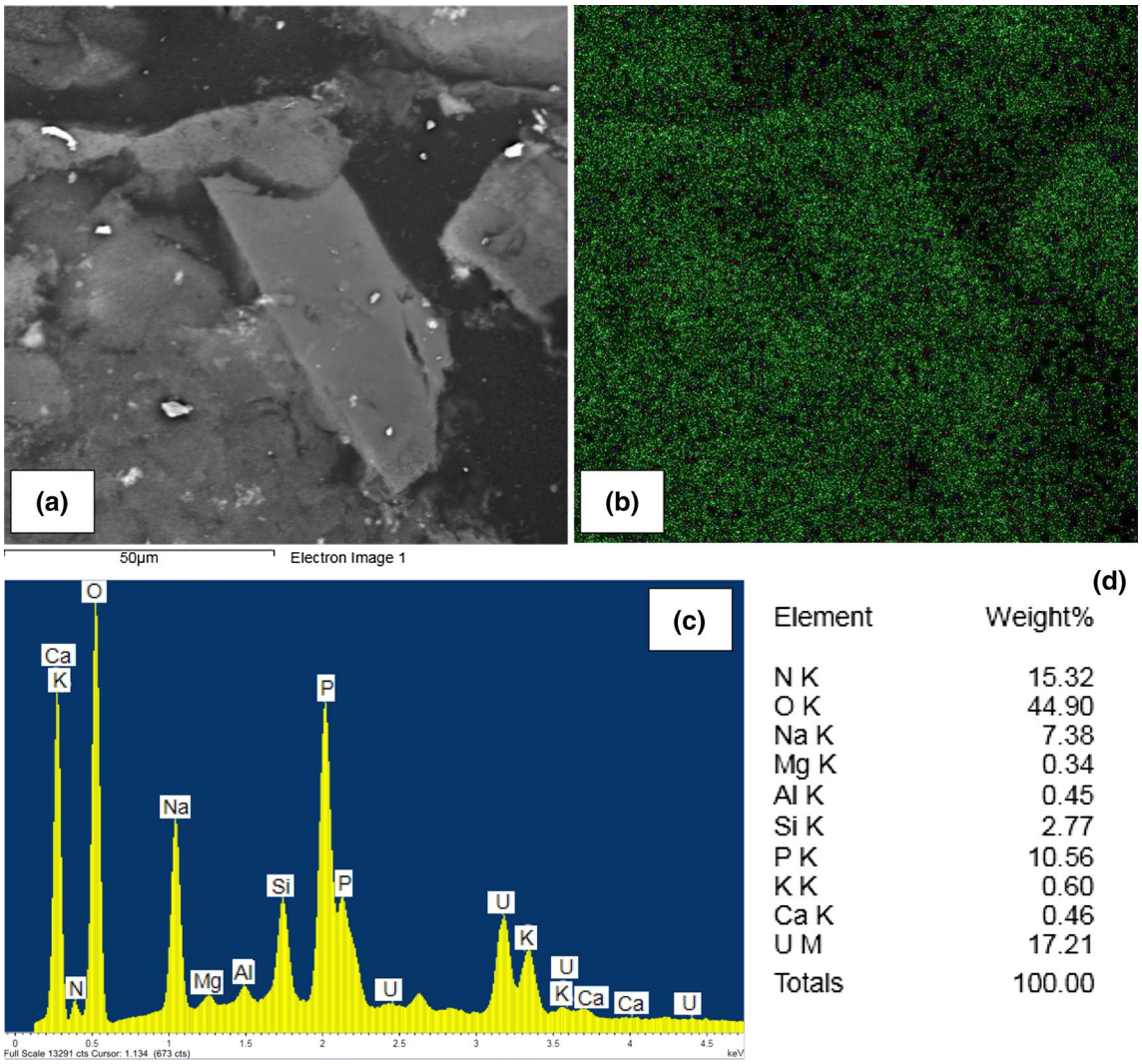

Fig. 6 SEM-BSE image of uranyl adsorbed Ch–V (**a**), EDX mapping analysis of Ch–V after adsorption of UO_2^{2+} (**b**), EDX spectrum of Ch–V after adsorption of UO_2^{2+} (**c**), Semi-quantitative EDX analysis of uranyl adsorbed Ch–V

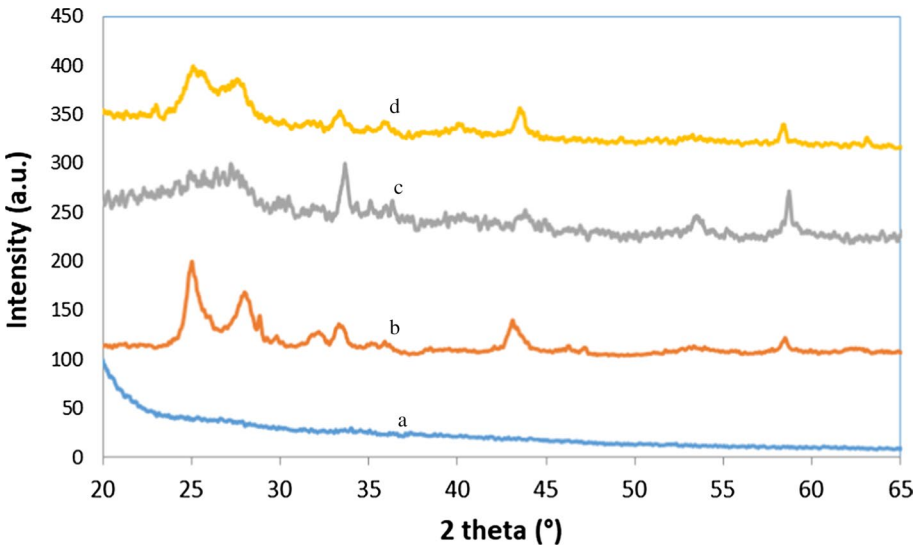

Fig. 7 XRD patterns of Ch (**a**), V (**b**), Ch–V (c) and uranyl adsorbed Ch–V (**d**)

was chosen for size fitting. Figure 7c is the XRD pattern of the chitosan-vermiculite composites with peaks related to vermiculite while a characteristic hump around 25° (2 theta) stands for chitosan. The vermiculite was estimated as a mixture of Grossite ($CaAl_4O_7$) and Margarite 2M1 which is Ca–Al–Si–OH related phase. These mixed phases were in 2 M monoclinic symmetry structure with layered structure of hydroxide and cations to be expanded up to 150% of longer dimension as being around 19 Å. The estimated primary crystallite size of chitosan-vermiculite composite was differentiated to be as 217 Å ± 15 Å. This may be a sufficient approval of expansion of vermiculite layers from 77 to 217 for organic structure to be intercalated in, as analyzed from 5 main peaks of vermiculite. UO_2^{2+} modified composite was represented in Fig. 7d. The peak separations at 26° and 28° at Fig. 7d may be associated to the adsorption of UO_2 by polymer-inorganic composites. The peak at 28.3° as a shoulder of the highest peak of vermiculite was found to be UO_2 [ICDD-PDF#41-1422] even at low concentration of adsorption which is attributed to higher atomic density in X ray diffraction. Since the adsorption of UO_2 is evident as valance exchange to be + 4, + 5, + 6 and + 7 to produce UO_2, U_2O_5 [ICDD-PDF#43-0111], UO_3 [ICDD-PDF#42-1140], U_3O_7 [ICDD-PDF#42-1215], respectively. Hence all U complexes are in different symmetries, the XRD scheme may not be totally clear. The crystallinity of composite as compared to Fig. 7c including chitosan with vermiculite, were increased by improved peak formation via lower background. The crystalline peak formation also means the decrease in Debye length size as to be 119 Å ± 5 Å. The smaller the height of peaks, the finer the Debye sizes. The interlayer expanding is much smaller than chitosan-vermiculite due to intercalation of UO_2 and a possible reaction with vermiculite and/or chitosan to bond the layers by larger atomic size.

Adsorption studies

Effect of pH on UO_2^{2+} adsorption and Determination of point of zero charge (PZC)

One of the most important factors affecting adsorption is the adsorbent surface charge which changes with the solution pH. For this reason, the surface charge must be determined. The most commonly used method for this, to measure initial pH and equilibrium pH for determining the PZC. Below the PZC the adsorbent surface is positively charged conversely, above PZC the adsorbent surface is negatively charged. The optimum conditions for UO_2^{2+} adsorption were determined using the surface charge density varied pH values. For this purpose, a series of experiments *were* performed to determine the PZC point of the newly synthesized composite. The obtained results were presented in Fig. 8. The experimental results were showed that the PZC point of the Ch–V was determined as 4.76. The surface charge of Ch–V was positive at pH < 4.76 and negative at pH > 4.76.

In order to investigate the pH effect, adsorption studies were carried out at different pHs at constant uranyl ion concentration and results are shown in Fig. 9. According to this

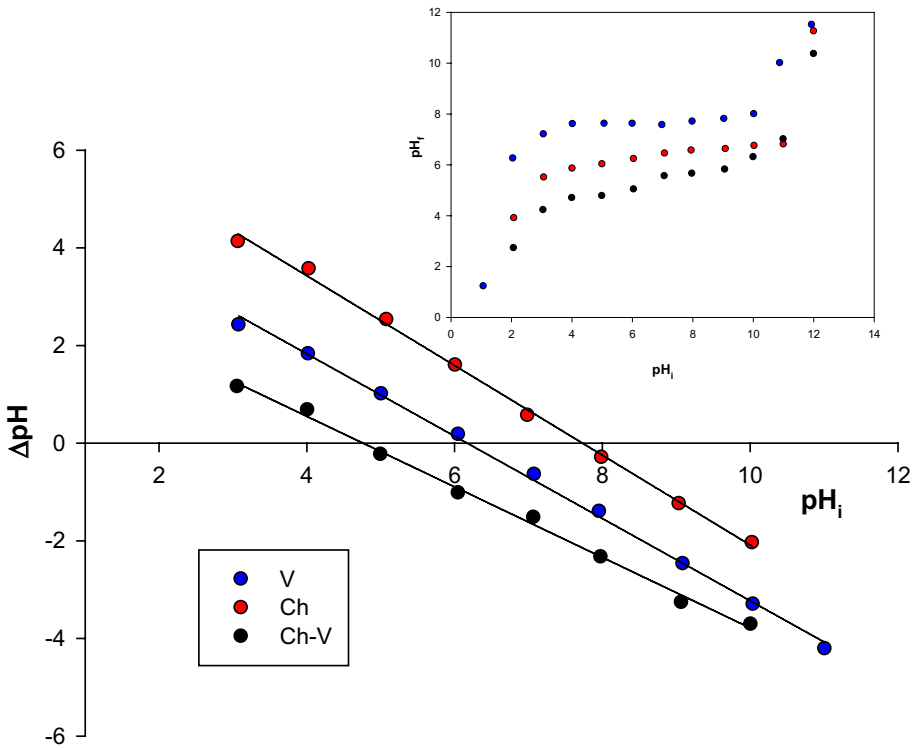

Fig. 8 PZC plots of adsorbent and its components

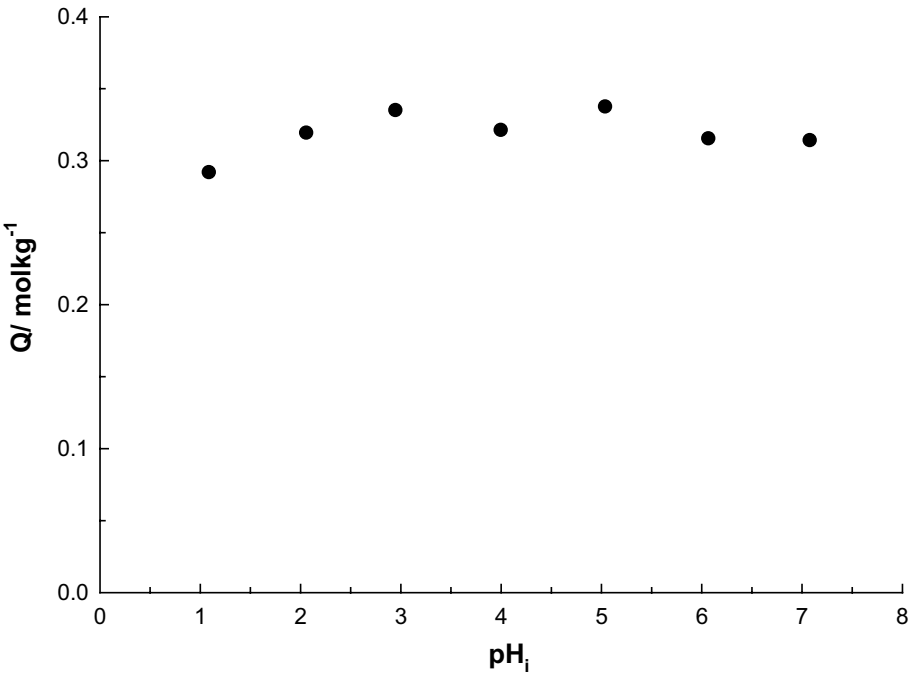

Fig. 9 Effect of pH on the adsorption {$[UO_2^{2+}]_0$: 1000 mg L^{-1}, adsorbent dosage:100 mg, V:10 mL, pH: 1.0–7.0, contact time: 24 h, temperature: 25 °C}

results, the pH of the solution did not cause a significant effect on uranyl ion adsorption. In the working range, UO_2^{2+} is the predominant species in the uranyl solution. There is no significant change under the 4.76 because of the both adsorbent and UO_2^{2+} surface charge does not change. Uranyl ions can precipitate at alkaline pHs as expected. So, it was not studied pHs beyond 7.0. At higher pHs than 7.0, UO_2^{2+} ions in the solution will precipitate and this will change structure and amount of uranyl ions in the solution such as such as $UO_2(OH)^+$, $UO_2(OH)_2^{2+}$ and $(UO_2)_3(OH)_5$ [21]. The presence of hydrolyzed uranyl species will cause a decrease in the UO_2^{2+} adsorption efficiency.

The adsorption mechanism for UO_2^{2+} ions of Ch–V composite beads may be estimated that the adsorptive active centers for UO_2^{2+} ions are at the amino groups and the hydroxyl groups in chitosan and the oxygen atoms in vermiculite. According to this, it can be concluded that the adsorption is carried out through the stronger electrostatic attraction or complex formation.

UO_2^{2+} adsorption

Although the adsorption process is an effective and applicable method, it is a highly complex process. Many chemical and physical factors such as heterogeneity of the surface, porosity, adsorbate-adsorbent interaction, energy changes, surface chemical structure and adsorbate surface affinity affect as thermodynamically and kinetically. Therefore, a single empirical model in the evaluation of the adsorption process is insufficient to explain all these factors. Adsorption isotherms can be easily explained using multiple models and parameters which provided from each model. For example, The Langmuir model accepts the surface homogeneous, which is the most suitable model for determining the maximum monolayer capacity of the adsorbent. Dubinin Radushkevich (D–R) model is used for more precise results for adsorption energy. Freundlich isotherm gives the most accurate information about surface heterogeneity. The change in adsorption of uranyl ions on Ch–V composite with concentration was investigated at five different temperatures. The obtained experimental data were fitted to Langmuir, Freundlich and D-R isotherm models.

The adsorption isotherms of uranyl ions on Ch–V composite and their compatibility to the Langmuir, Freundlich, D–R models were compared in Fig. 10, and the parameters found in these models were given in Table 2. The uranyl adsorption results of the composite showed that the composite has a very high adsorption capacity. When the adsorbents based on the components are compared to the newly synthesized adsorbent composite, it is shown that it can be used in the recovery and enrichment works of uranium with both adsorption capacity and ease of use. Vermiculite is a natural mineral which can be used as a pure adsorbent depends on its content. But, it is not useful due to its disadvantages on pH. The vermiculite consists of silicates and other clay minerals. When increases the pH to alkaline conditions, this situation especially causes precipitation of the absorbed metals as metal hydroxides. Due to the hydrolysis of chitosan under alkaline conditions and dissolution in acidic conditions, it is unsuitable to use as pure adsorbent. It has been shown that the newly synthesized composite material can be used as an adsorbent by eliminating these properties by means

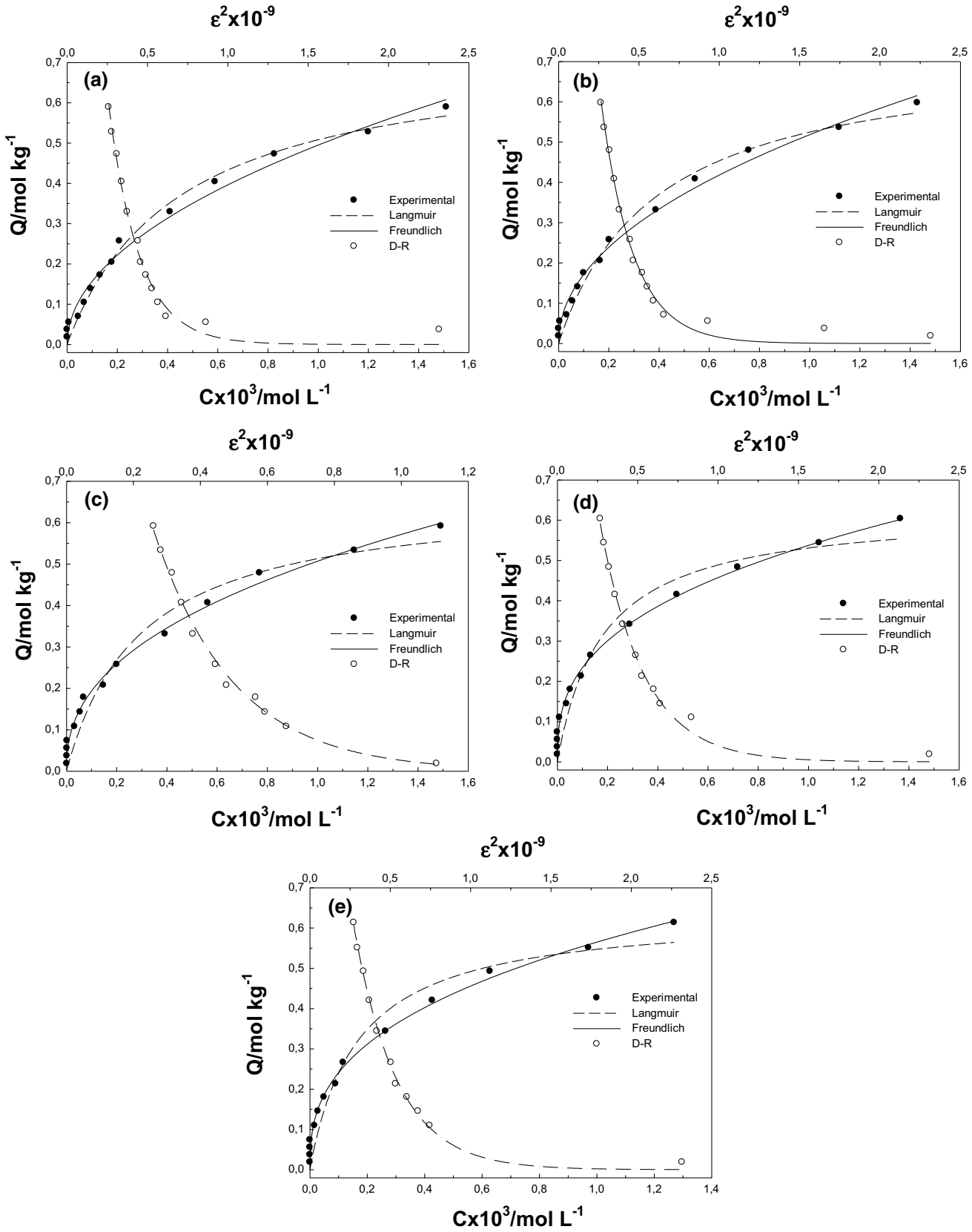

Fig. 10 Effect of temperature on the adsorption isotherms for UO_2^{2+} onto Ch–V at **a** 5 °C, **b** 15 °C, **c** 25 °C, **d** 40 °C, **e** 50 °C. {$[UO_2^{2+}]_0$:50–2000 mg L^{-1}, adsorbent dosage:100 mg, V:10 mL, natural pH:4.0–4.5, contact time:24 h}

Table 2 Adsorption equilibrium parameters for the adsorption of UO_2^{2+} onto Ch–V

	5 °C	15 °C	25 °C	40 °C	50 °C
Langmuir					
K_L (L mol^{-1})	2243	2586	3376	5548	6008
X_m (mol kg^{-1})	0.735	0.727	0.665	0.627	0.638
R^2	0.988	0.985	0.960	0.948	0.955
Freundlich					
K_F	15.5	14.4	9.08	6.51	7.28
n	0.499	0.481	0.472	0.361	0.370
R^2	0.986	0.990	0.993	0.982	0.982
DR					
X_{DR}	2.31	2.24	1.86	1.58	1.68
$-K_{DR}$x10^9	5.22	4.98	4.39	3.68	3.73
R^2	0.990	0.992	0.995	0.994	0.997
E/kJ mol^{-1}	9.78	10.0	10.7	11.7	11.6

Table 3 Adsorption kinetic parameters for UO_2^{2+} removal using Ch–V as adsorbent

	C_0, 1000 mg L^{-1}
Pseudo first order	
Q_t (mol kg^{-1})	0.338
Q_e (mol kg^{-1})	0.331
$k_1 \times 10^3$ (dk^{-1})	21.3
$H \times 10^3$ (mol kg^{-1} min^{-1})	7.06
R^2	0.987
Pseudo second order	
Q_t (mol kg^{-1})	0.338
Q_e (mol kg^{-1})	0.371
$k_2 \times 10^3$ (mol^{-1} kg min^{-1})	1.39
$H \times 10^3$ (mol kg^{-1} min^{-1})	0.983
Intraparticle diffusion model	
$k_i \times 10^3$ (mol kg^{-1} min$^{-0.5}$)	15.5
R^2	0.959

of its components. The parameters used in the isotherms are given in the Table 2. The maximum adsorption capacity from the Langmuir model is quite high as 0.665 mol kg^{-1} at 25 °C. The Freundlich parameter n indicates the degree of heterogeneity of the surface, and the E_{DR} value found in the DR model indicates that the adsorption is chemical. If the E_{DR} value is between 8 and 16 kjmol^{-1}, it is considered as chemical adsorption.

Adsorption kinetics

One of the important parameters of the adsorption process is to know the adsorption time. Prediction of the completion time of adsorption is main both for the kinetic control of the process and renewal of the adsorbent. In this respect, design of high adsorbents became importance. Adsorption is considered as a sum of different kinds of events that occur together or sequentially between the adsorbent and the adsorbate. Among these, events such as the transfer of ions to the adsorbent surface in the solution, the formation of film on the surface, the filling of the surface pores, the diffusion of the particles inside the particle diffusing into the particle are the predictive factors in determining the time of adsorption. As a result, since the adsorption range is not clear, the determination of the rate of adsorption and the rate of adsorption velocity will be possible only by investigating the compatibility of experimental results to different kinetic models [22]. Kinetic models used in adsorption studies and applied to description the adsorption kinetics such as pseudo first order (PFO), pseudo second order (PSO) and intraparticle diffusion (IPD) models were used in this study, the equations and the parameters (Table 3) found in the related equations are shown in Fig. 11.

Regression coefficients, which are a measure of the harmony of adsorption to kinetic models, are used to determine the appropriate model. The affinity of the Q_e values to the experimental Q_e values is more accurate for determining the appropriate model. In this respect, the PSO model is a suitable model for the adsorption kinetics of uranyl ions on the Ch–V adsorbent. Additionally, the PSO model is a more accurate model for explaining the adsorption kinetics under the adsorption conditions with low initial concentrations. Even if the regression coefficient is high, the PFO model is valid in adsorption processes with high initial concentrations. The PSO model predicts the rate of adsorption through diffusion. However, with surface diffusion in adsorption, it plays an active role in diffusion into the particle. The multilinearity of the experimental results to the IPD model showed that the diffusion of the particle is important in kinetic terms. When the two models are evaluated together, velocity on adsorption of uranyl ions on to the new adsorbent is determined by rapid diffusion of surface with relatively slower particle diffusion.

Effect of temperature on the adsorption and thermodynamic parameters

The thermodynamic parameters of the adsorption process were calculated at five different temperatures (Fig. 12). By using the equations given in Table 4 the obtained results presented in Table 4. K_L values are used by applying Langmuir model to the isotherms which were created at different temperatures in order to find the thermodynamic parameters [23]. Thermodynamic parameters such as, enthalpy (ΔH^0), entropy (ΔS^0) and free energy values were calculated to investigate the effect of temperature on adsorption, results

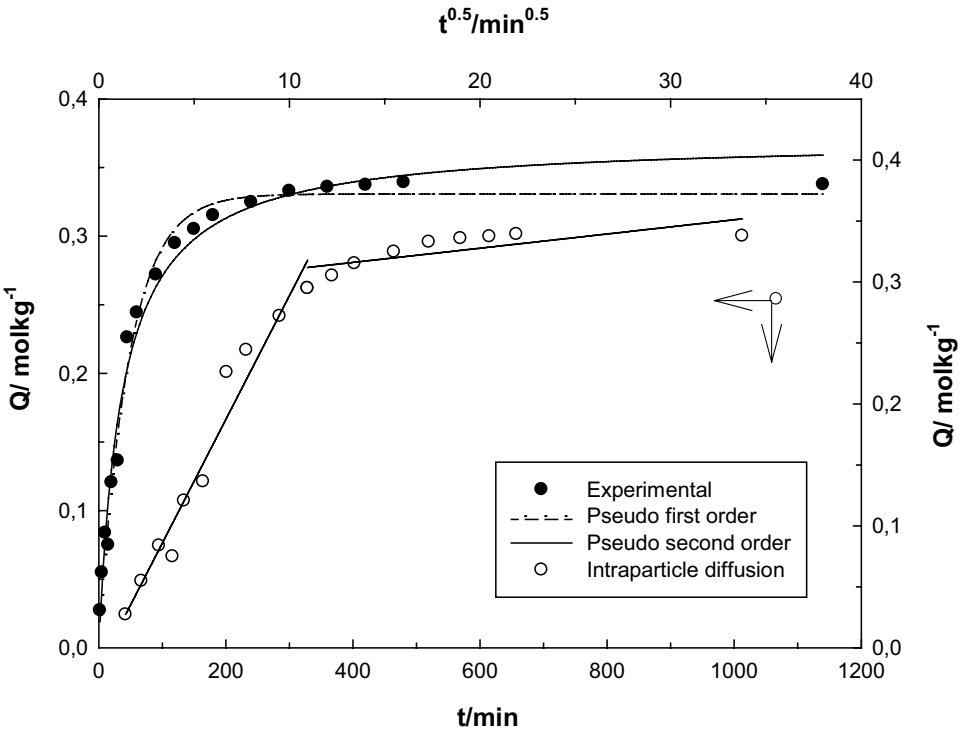

Fig. 11 Compatibility of UO_2^{2+} adsorption kinetics to pseudo-first-order, pseudo-second-order and intra-particle diffusion models. {$[UO_2^{2+}]_0$: 1000 mg L^{-1}, adsorbent dosage:300 mg, V:30 mL, natural pH:4.0–4.5, contact time:24 h, temperature:25 °C}

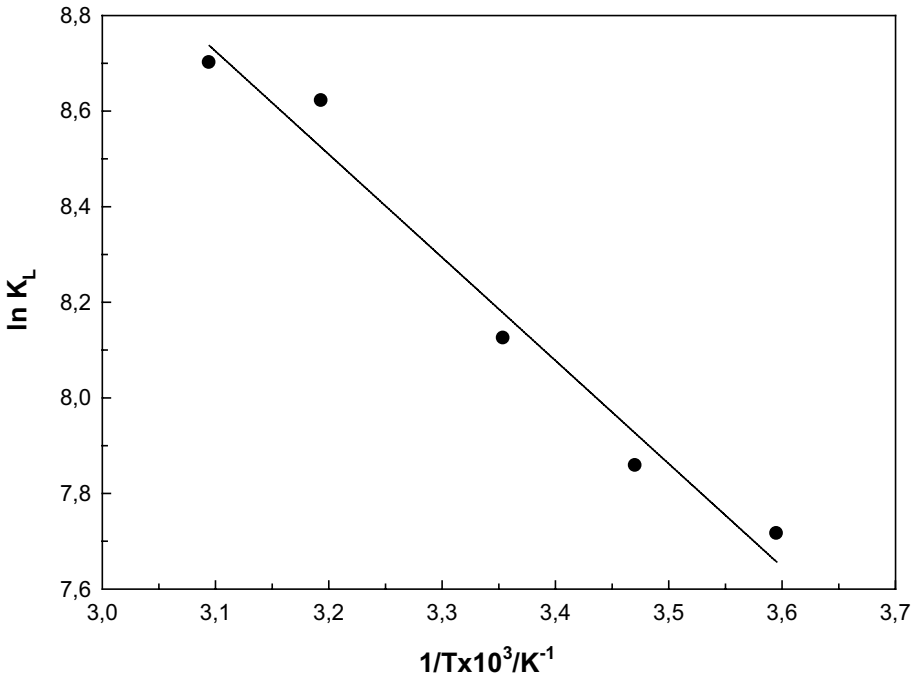

Fig. 12 The effect of temperature on the adsorption of UO_2^{2+} onto Ch–V. {$[UO_2^{2+}]_0$: 1000 mg L^{-1}, adsorbent dosage:100 mg, V:10 mL, natural pH:4.0–4.5, contact time:24 h, temperature: 5 °C, 15 °C, 25 °C, 40 °C, 50 °C}

and equations are presented in Table 4. Adsorption enthalpy was found positive. The positive adsorption enthalpy indicates that energy is consumed during the adsorption process. Due to the nature of the adsorption, entropy is expected to decrease. However, the adsorption entropy is not only the adsorption entropy but also the entropy of the whole process. Dehydration, separation of water molecules, events between the solid-phase and the solution-phase such are played a key role between the entropy-enhancing events. Their contribution to entropy causes increase in the whole process. During the adsorption process, randomness has increased in all the system. The free enthalpy value is negative and as expected spontaneity. Moreover, the value of DR model indicates the adsorption mechanism, which is chemical or physical.

Table 4 Thermodynamic parameters of adsorption

	5 °C	15 °C	25 °C	40 °C	50 °C
K_L (L mol^{-1})	2243	2586	3376	5548	6008
ΔG (kJ mol^{-1})	− 17.7	− 18.9	− 20.3	− 22.1	− 23.4
ΔS^0 (J mol^{-1} K^{-1})			128		
ΔH^0 (kJ mol^{-1})			17.9		
R^2			0.972		

When this value evaluated with the thermodynamic data, the adsorption event is chemical. From this result, it can be concluded that the adsorption is carried out through ion exchange, chelate formation or stable complex.

The effect of ionic strength on adsorption

In order to investigate the effect of ionic strength on adsorption, a series experiments were performed with constant uranyl ion solutions at different KNO_3 concentrations. The obtained results were given in Fig. 13. Increasing the ionic strength can affect the competition of cations such as Na^+, K^+ and other adsorbed molecules, besides it changes the "saline effect" or "ionic atmosphere", which affects the adsorption. Most studies have shown that ionic strength does not affect or increase the adsorption, while inner surface affects the formation of complex whereas increase in ionic strength can be explained by the outer surface [24]. In this study, the results showed that the effect of ionic strength on adsorption did not cause quantifiable changes. This result explains that the adsorption takes place over the inner surface complexes. The lower effect of ionic strength on the adsorption was indicated that there is no effect of ion exchange. In addition, the formation of the complex shows that the adsorption is chemical.

Recovery

The conditions of adsorption/desorption uranyl ions on adsorption by composite were investigated using different solutions. Recovery studies were carried out via different solutions in order to strip uranyl ions on adsorbent surface. After 1000 mg L^{-1} of uranyl, the solution was equilibrated with 100 mg adsorbent solid phase was removed. Then, desorption of adsorbed ions was activated using HCl, NaOH, HNO_3 and ethyl alcohol solutions (each one, 0.1 mol L^{-1}). The uranyl ions in stripping solutions were determined spectrophotometrically. Results of this study were presented in Fig. 14, the experiments were repeated three times with the same adsorbent for the adsorption/desorption cycle. The highest recovery was achieved by HCl (79%) whereas the ethyl alcohol (2%) was very low. This result showed that the adsorption of uranyl ions is chemical.

Conclusion

This study showed that, for the first-time, that Ch–V composite beads synthesized using vermiculite and chitosan beads, which could effectively remove uranyl ions from

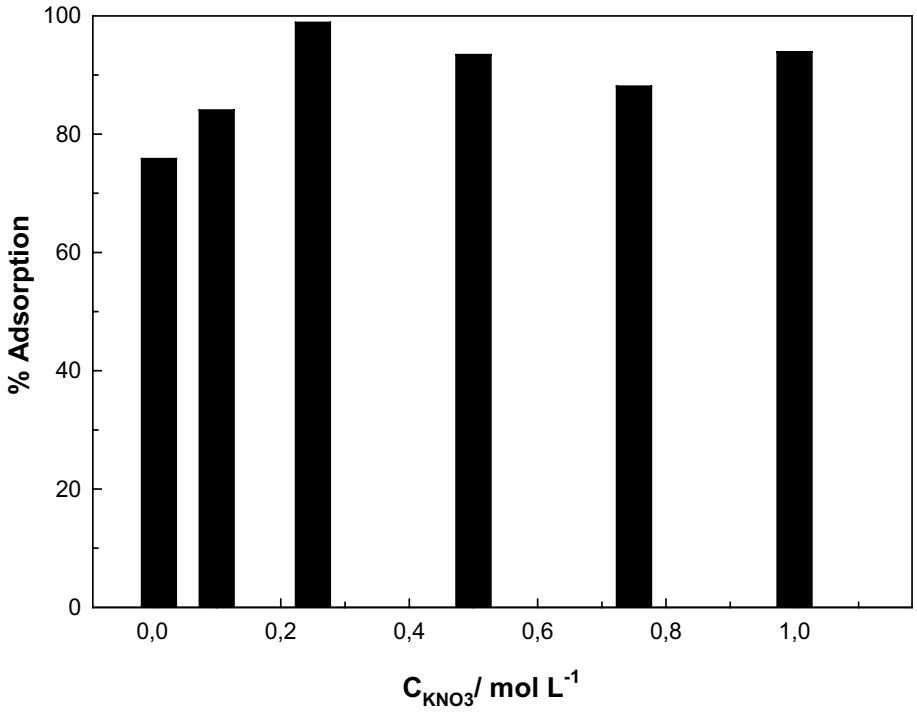

Fig. 13 The effect of ionic strength on the adsorption of UO_2^{2+} onto Ch–V. {[UO_2^{2+}]$_0$:1000 mg L^{-1}, adsorbent dosage:100 mg, V:10 mL, natural pH:4.0–4.5, contact time:24 h, temperature:25 ^{0}C}

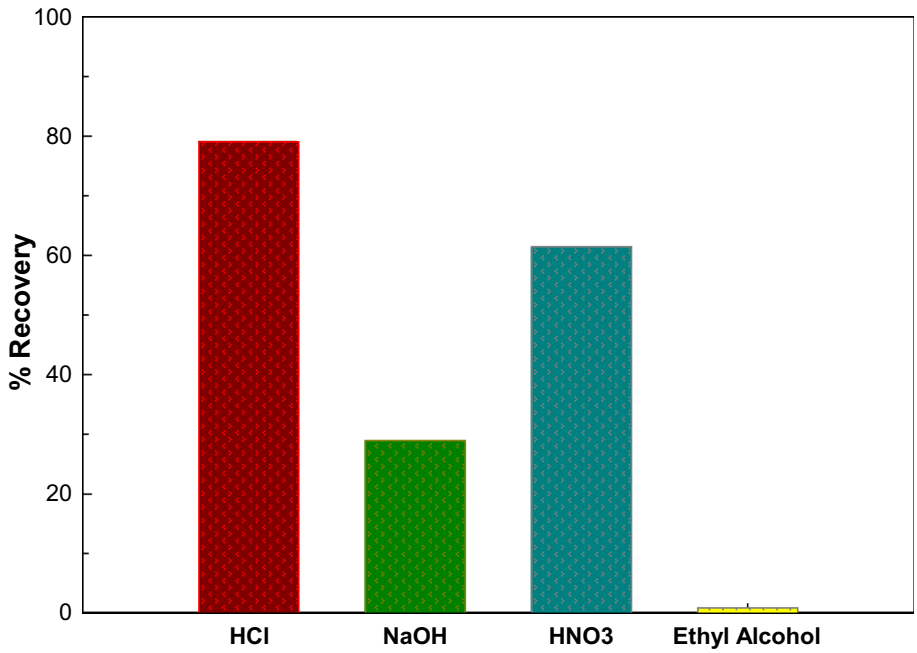

Fig. 14 Recovery percent of various solvent for desorption of uranyl ions. {$[UO_2^{2+}]_0$: 1000 mg L^{-1}, adsorbent dosage:100 mg, V:10 mL, natural pH:4.0–4.5, contact time:24 h, temperature:25 °C}

the aqueous solution. The structural analysis results of new composite showed that the composite is different from the own components. All parameters affecting the removal of hexavalent uranium from aqueous solution were investigated and optimum conditions were determined in detailed. All obtained results showed that newly developed Ch–V composite can be actively used as adsorbent with high capacity with the purpose of removal or recovery of uranyl ions. Moreover, It is an environmental friendly, effective and cheap adsorbent. The adsorption capacity of chitosan based on composites reported in literature, some selected studies are presented in Table 5. As can be seen in this table, the maximum adsorption capacity of newly synthesized Ch–V composite is higher than most adsorbents reported so far. It also has a potential to be used effectively for removal of other toxic species from the aqueous medium.

Table 5 Adsorption capacities of various chitosan based composites

Adsorbent	Adsorption capacities/ mgg^{-1}	References
Chitosan/PVA	156	[25]
Magnetic chitosan	666.67	[26]
Magnetik amidoximated chitosan	117.65	[27]
Magnetic hydrothermal cross-linking chitosan	404.50	[28]
Carboxymethylated chitosan/Na-bentonite	115.60	[29]
Polydopamine-functionalized attapulgite/chitosan	165.60	[30]
Chitosan/polyaniline composite	204.08	[31]
Nano-ZnO/Chitosan Bio-composite Beads	148.70	[32]
Chitosan@attapulgite	53.50	[33]
Chitosan modified phosphate rock	8.67	[34]
Magnetic chitosan/graphene oxide nanocomposites	178.60	[35]
Chitosan impregnated Ca-alginate	36.04	[36]
Chitosan–Vermiculite beads	179.6	This study

Acknowledgements The present study was partly supported by Cumhuriyet University Scientific Research Projects Commission.

Compliance with ethical standard

Conflict of interest The authors strongly declare that no scientific and/or financial conflicts of interest, exists with other people or institutions.

References

1. Keith LS, Faroon OM, Fowler BA (2007) Uranium. İn: Berlin M, Zalups RK, Fowler BA (eds) Handbook on the toxicology of metals. Academic Press, Copenhagen, pp 880–903
2. Crini G, Lichtfouse E (2019) Advantages and disadvantages of techniques used for wastewater treatment. Environ Chem Lett 7:145–155
3. Gisi SD, Lofrano G, Grassi M, Notarnicola M (2016) Characteristics and adsorption capacities of low-cost sorbents for wastewater treatment: a review. Sustain Mater Techn 9:10–40
4. Luo M, Liu S, Li J, Luo F, Lin H, Yao P (2016) Uranium sorption characteristics onto synthesized pyrite. J Radioannal Nucl Chem 307:305–312
5. Zhu R, Chena Q, Zhoua Q, Xi Y, Zhua J, He H (2016) Adsorbents based on montmorillonite for contaminant removal from water: a review. Appl Clay Sci 123:239–258
6. Simsek S, Ulusoy U (2013) Adsorptive properties of sulfolignin–polyacrylamide graft copolymer for lead and uranium: effect of hydroxilamine–hydrochloride treatment. React Funct Polym 73:73–82
7. Moghaddam RH, Dadfarnia S, Shabani AMH, Tavakol M (2019) Synthesis of composite hydrogel of glutamic acid, gum tragacanth, and anionic polyacrylamide by electron beam irradiation for uranium (VI) removal from aqueous samples: equilibrium, kinetics, and thermodynamic studies. Carbohydr Polym 206:352–361
8. Salehi E, Daraei P, Shamsabadi AA (2016) A review on chitosan-based adsorptive membranes. Carbohydr Polym 152:419–432
9. Kotal M, Bhowmick AK (2015) Polymer nanocomposites from modified clays: recent advances and challenges. Prog Polym Sci 51:127–187
10. Malandrino M, Abollino O, Giacomino A, Aceto M, Mentasti E (2006) Adsorption of heavy metals on vermiculite: influence of pH and organic ligands. J Colloid Interf Sci 299:537–546
11. Rinaudo M (2006) Chitin and chitosan: properties and applications. Prog Polym Sci 31:603–632
12. Zhang L, Zeng Y, Cheng Z (2016) Removal of heavy metal ions using chitosan and modified chitosan: a review. J Mol Liq 214:175–191
13. Simsek S, Senol ZM, Ulusoy HI (2017) Synthesis and characterization of a composite polymeric materialincluding chelating agent for adsorption of uranyl ions. J Hazard Mater 338:437–446
14. Chen L, Wu P, Chen M, Lai X, Ahmed Z, Zhu N, Dang Z, Bi Y, Liu T (2018) Preparation and characterization of the eco-friendly chitosan/vermiculite biocomposite with excellent removal capacity for cadmium and lead. Appl Clay Sci 159:74–82
15. Saleh TA, Sarı A, Tuzen M (2016) Chitosan-modified vermiculite for As (III) adsorption from aqueous solution: equilibrium, thermodynamic and kinetic studies. J Mol Liq 219:937–945
16. Padilla-Ortega E, Darder M, Aranda P, Gouveia RF, Leyva-Ramos R, Ruiz-Hitzky E (2016) Ultrasound assisted preparation of chitosan–vermiculite bionanocomposite foams for cadmium uptake. Appl Clay Sci 130:40–49
17. Prakash N, Soundarrajan M, Vendan SA, Sudha PN, Renganathan NG (2017) Contemplating the feasibility of vermiculate blended chitosan for heavy metal removal from simulated industrial wastewater. Appl Clay Sci 7:4207–4218
18. Long H, Wua P, Yang L, Huang Z, Zhu N, Hu Z (2014) Efficient removal of cesium from aqueous solution with vermiculite of enhanced adsorption property through surface modification by ethylamine. J Colloid Interf Sci 428:295–301
19. Prakash N, Soundarrajan M, Vendan Arungalai S, Sudha PN, Renganathan NG (2017) Contemplating the feasibility of vermiculate blended chitosan for heavy metal removal from simulated industrial wastewater. Appl Water Sci 7:4207–4218
20. Zheng Y, Li P, Zhang J, Wang A (2007) Study on superabsorbent composite XVI Synthesis, characterization and swelling behaviors of poly(sodium acrylate)/vermiculite superabsorbent composites. Eur Polym J 43:1691–1698
21. Ilaiyaraja P, Ashish Kumar Singh D, Sivasubramanian K, Ponraju D, Venkatraman BI (2013) Adsorption of uranium from aqueous solution by PAMAM dendron functionalized styrene divinylbenzene. J Hazard Mater 251:155–166
22. Lima EC, Adebayo MA, Machado FM (eds) (2015) Kinetic and equilibrium models of adsorption CP Bergmann. Springer, New York, pp 33–69
23. Lima EC, Hosseini-Bandegharaei A, Moreno-Piraján JC, Anastopoulos I (2019) A critical review of the estimation of the thermodynamic parameters on adsorption equilibria wrong use of equilibrium constant in the Van't Hoof equation for calculation of thermodynamic parameters of adsorption. J Mol Liq 273:425–434
24. Zhiwei N, Qiaohui F, Wenhua W, Junzheng X, Lei C, Wangsuo W (2009) Effect of pH, ionic strength and humic acid on the sorption of uranium(VI) to attapulgite. Appl Radiat Isot 9:1582–1590
25. Liu Y, Cao X, Hua R, Wang Y, Liu Y, Pang C, Wang Y (2010) Selective adsorption of uranyl ion on ion-imprinted chitosan/PVA cross-linked hydrogel. Hydrometallurgy 104:150–155
26. Hritcu D, Humelnicu D, Dodi G, Popa MI (2012) Magnetic chitosan composite particles: evaluation of thorium and uranyl ion adsorption from aqueous solutions. Carbohydr Polym 87:1185–1191
27. Zhuang S, Cheng R, Kang M, Wang J (2018) Kinetic and equilibrium of U(VI) adsorption onto magnetic amidoxime-functionalized chitosan beads. J Clean Prod 188:655–661
28. Yu SL, Dai Y, Caol XH, Zhang ZB, Liu YH, Ma HJ, Xiao SJ, Lai ZJ, Chen HJ, Zheng Z, Le ZG (2016) Adsorption of uranium(VI) from aqueous solution using a novel magnetic hydrothermal cross-linking chitosan. J Radioannal Nucl Chem 310:651–660
29. Zhou L, Ouyang J, Shehzad H, Le Z, Li Z, Adesina AA (2018) Adsorption of U(VI) onto the carboxymethylated chitosan/Nabentonite membranes: kinetic, isothermic and thermodynamic studie. J Radioannal Nucl Chem 317:1377–1385
30. Liao Y, Wang M, Chen D (2018) Production of three-dimensional porous polydopamine-functionalized attapulgite/chitosan aerogel for uranium(VI) adsorption. J Radioannal Nucl Chem 316:635–647
31. Liu J, Zhao C, Yuan G, Dong Y, Yang J, Li F, Liao J, Yang Y, Liu N (2018) Adsorption of U(VI) on a chitosan/polyaniline composite in the presence of Ca/Mg-U(VI)-CO_3 complexes. Hydrometallurgy 175:300–311
32. Kaynar UH, Cınar S, Cam Kaynar S, Ayvacıklı M, Aydemir T (2018) Modelling and optimization of uranium (VI) ions adsorption onto nano-ZnO/chitosan bio-composite beads with response surface methodology (RSM). J Polym Environ 26:2300–2310
33. Pan D, Fan Q, Fan F, Tang Y, Zhang Y, Wu W (2017) Removal of uranium contaminant from aqueous solution by chitosan@attapulgite composite. Sep Purif Technol 177:86–93
34. Sun Z, Chen D, Chen B, Kong L, Su M (2018) Enhanced uranium(VI) adsorption by chitosan modified phosphate rock. Colloids Surf A 547:141–147

35. Huang G, Peng W, Yang S (2018) Synthesis of magnetic chitosan/graphene oxide nanocomposites and its application for U(VI) adsorption from aqueous solution. J Radioannal Nucl Chem 317:337–344
36. Basu H, Singhal RK, Saha S, Pimple MV (2017) Chitosan impregnated Ca-alginate: a new hybrid material for removal of uranium from potable water. J Radioannal Nucl Chem 314:1905–1914